ISTITUTO NAZIONALE DI GEOFISICA E VULCANOLOGIA

ACCEPTED ON ANNALS OF GEOPHYSICS, 61, 2018; Doi: 10.4401/ag-7788

Latitudinal dependence of geomagnetically induced currents during geomagnetic storms

Roberta Tozzi, Igino Coco, Paola De Michelis, Fabio Giannattasio

Istituto Nazionale di Geofisica e Vulcanologia, Roma, Italy

Latitudinal dependence of geomagnetically induced currents during geomagnetic storms

ROBERTA TOZZI*, IGINO COCO, PAOLA DE MICHELIS, FABIO GIANNATTASIO

Istituto Nazionale di Geofisica e Vulcanologia

Via di Vigna Murata 605, 00143 Roma, Italia

*Corresponding author: email: roberta.tozzi@ingv.it, telephone: +39 0651860389, fax: 51860397

Abstract

Major geomagnetic storms drive rapid intensification and variability of magnetospheric and ionospheric current systems that give rise to large ground-induced currents (GIC). Space weather associated GIC pose a serious threat to the reliability of power-transmission systems and other electrically conducting infrastructure such as oil and gas pipelines. The most severe effects are observed at high latitudes due to ionospheric currents associated with the aurora. However, as power transmission grid and pipeline infrastructure continues to grow at middle and low-latitudes, GIC hazards are no longer just concerns of high-latitude regions. We investigate how GIC amplitude varies in latitude during six major geomagnetic storms that occurred between 1989 and 2004. Due to limited direct GIC measurements, a proxy of the geoelectric field is used, i.e. the GIC index. This is calculated for the selected geomagnetic storms using 25 magnetic observatories relatively uniformly distributed in geomagnetic latitude, 14 magnetic observatories with longitudes varying within a range of 45 degrees as well as for the 7 November 2004 storm using 104 observatories. In addition, we suggest a possible way to follow the latitudinal displacement of the auroral oval during geomagnetic storms through the maximum value of GIC index, estimated over 2-hour intervals on a wide number of magnetic observatories.

Keywords: geomagnetically induced currents, magnetic field data, space weather

I. INTRODUCTION

Large-scale time-varying currents flowing in the ionosphere and magnetosphere are responsible for the origin of electric and magnetic fields at the Earth's surface. Specifically, electric currents are induced in the conductive ground when particularly intense and rapid variations occur in the ionospheric and magnetospheric current systems due to perturbations of solar origins. These currents, known as geomagnetically induced currents (GIC), can flow through infrastructure networks such as railroads, power transmission lines, and pipelines with damages ranging from the slow degradation to the immediate manifestation of ruptures and malfunctioning [Ngwira & Pulkkinen, 2018]. A well-known example of the possible damages inflicted by GIC is the collapse of the Canadian power grid of the entire Hydro-Québec occurred during the geomagnetic storm of October 1989. On that occasion a

blackout followed, affecting more than 6 million people and the Québec province was submerged in darkness for more than nine hours. This episode has taught a lot about the potential vulnerability of the most critical ground-based infrastructures to space weather events and, since then, a lot of scientific efforts have been devoted to gain a better comprehension of this phenomenon.

Since the origin of GIC are the electric currents flowing overhead, the nearer and stronger the currents, the more dramatic their effects. It follows that currents flowing in the ionosphere at polar latitudes (e.g. auroral electrojects) are among the most important sources of GIC. These currents flow about a hundred kilometres away from the Earth's surface and, during geomagnetically disturbed periods, can reach intensities up to 4-5 times their quiet time values, thus giving rise to wide and rapid geomagnetic field variations going from hundreds to thousands nanoTeslas [Smith et al., 2017]. Moreover, under deeply perturbed conditions the position of the auroral oval can consistently move towards lower latitudes posing a GIC risk also for middle latitudes countries. There are other possible GIC sources that cannot be neglected [Pulkkinen et al., 2012; Ngwira et al. 2013; Carter et al., 2015], i.e. the equatorial electrojet (EEJ) and ring current. Despite both these currents produce, for different reasons, signatures on the geomagnetic field that are less evident than those produced by the polar current systems, there are many proofs of their effects at middle and low latitudes. Just to mention a few examples: the damages to some South African transformers occurred during the October 2003 geomagnetic storm [Gaunt & Coetzee, 2007], those on transformers of a power line system in Hokkaido [Watari et al., 2009] or on the New Zealand's South Island power network during the moderate storm of 7 November 2001 [Marshall et al., 2012].

The mechanisms for the generation of GIC are still unclear, especially concerning middle and low latitudes and diverse hypotheses have been proposed. A dominant idea is that the occurrence of the most intense GIC relates to sudden impulses or sudden storm commencements sometimes preceding a geomagnetic storm [e.g. Fiori et al., 2014; Carter et al., 2016]. These impulses are produced by the increase of magnetopause currents following the compression of the magnetosphere by the plasma expelled from the Sun during solar phenomena as coronal mass ejections or corotating interaction regions [Adebesin et al., 2016]. Other authors have found that at middle latitudes large voltages can be also observed during the recovery phase of geomagnetic storms and are due to Pc5 pulsations [Hejda & Bochníček, 2005]. Besides the strength of the sources producing geomagnetic field variations, an important role is played also by ground conductivity that can produce very high local intensifications of GIC, thus complicating the understanding of this phenomenon. For instance, the amplification of electric currents that led to the dramatic blackout occurred in 1989 in Canada was due also to Québec's position on a large low-conductivity rock shield that prevented the current from flowing through the earth [Lotko, 2017], under this circumstance the electric current finds a less resistant path along the power lines.

During the last decades, the increasing dependence on technology of society has renewed the interest in the investigation of the mechanisms and phenomenology of GIC that are undoubtedly a source of vulnerability to man-made infrastructures due to Earth-directed space weather events. It has been estimated that in the United States and Canada the vulnerability of critical infrastructures to space weather impacts was almost tripled in only twenty years [Molinski, 2002]. Also equatorial countries are becoming increasingly susceptible to space weather impacts as a consequence of the effects that intensifications of the stormtime EEJ [Ngwira et al., 2013] can have on the rapidly developing transnational power grids [Moldwin & Tsu, 2016].

The characterization of geomagnetic latitudes based on different risk levels associated with space weather impacts is among one of the open issues in this field. Such a classification could help countries in taking appropriate protection actions. Pulkkinen et al. [2012] investigated how the geoelectric field, computed using geomagnetic field data and ground conductivity estimates, changed with geomagnetic latitude during the storms of March 1989 and October 2003. They showed that the geoelectric field magnitudes may go through a steep drop at geomagnetic latitudes of about 40°– 60°and suggested that further analyses were required to confirm the existence and location of a possible "latitude threshold boundary", below which the risk associated with GIC can be considered negligible. Using an extended set of geomagnetic storms Ngwira et al. [2013] reconstructed the latitudinal profile of the maximum GIC amplitude and found that most intense GIC are due to auroral electrojets but that the EEJ, too, is responsible for the enhancement of GIC intensity. Ngwira et al. [2013] used, as a proxy for GIC intensity, the amplitude of the geoelectric field estimated by means of the plane wave method [Pirjola, 1982] and the Québec ground conductivity model.

In this paper we reconstruct the latitudinal profile of the maximum GIC amplitude by means of the so-called *GIC* index [Marshall et al., 2010, 2011] as an alternative to the methods previously used. We first select two sets of magnetic observatories, approximately uniformly spaced in geomagnetic latitude, and study how the maximum intensity of GIC changes with latitude during six intense geomagnetic storms. One set consists of 25 magnetic observatories with longitudes spanning the entire 0°-360° range. The other set consists of 14 magnetic observatories with longitudes varying within 45 degrees. The use of this small set of observations has the purpose to consider the localized in local time nature of many of the current systems developing during geomagnetically disturbed conditions. As shown in detail by Tsuji et al. [2012], the local time location of the observatory at the universal time (UT) of a storm has a large impact on the amplitude of the measured perturbation. As a further analysis we choose the geomagnetic storm of November 2004 and go more in depth using, this time, data from around a hundred magnetic observatories and study the time variation of *GIC* index latitudinal profile with a sampling of two hours.

The paper is organised as follows. After a thorough description of data selection, *GIC* index is introduced also through a few examples. Then, *GIC* index is estimated for both the cases of the reduced and extended sets of magnetic observatories and results described and discussed. Finally, main conclusions are summarised.

II. DATA

Our analysis is based on the assumption that GIC intensity can be well represented by the *GIC* index introduced by Marshall et al. [2010, 2011] and explained in detail in the next section. The choice to use a proxy of the geoelectric field, and hence of GIC intensity, instead of their real measurements, is a consequence of the global character of the study here proposed. Indeed, real GIC measurements are very difficult to be retrieved on a local scale already, even more on a global scale. Moreover, even if these data were available, they would very likely be inhomogeneous and patchy. Also, the temporal coverage would leave a lot to be desired. The situation is quite different for *GIC* index that, as it will be shown in what follows, can be rather straightforwardly estimated by 1-minute values of the Northward (X) and Eastward (Y) Cartesian components of the geomagnetic field collected at ground magnetic observatories. These, in most cases, follow well-defined standards concerning instrumentation, measuring techniques as well as observatory practice in general. INTERMAGNET observatories follow such strict standards [Love & Chulliat, 2013]. INTERMAGNET constitutes a global network of observatories for monitoring the Earth's magnetic field that adopts "modern standard specifications for measuring and recording equipment", as well as for data processing, "in order to facilitate data exchanges and the production of geomagnetic products in close to real time" (citation from www.intermagnet.org).

First of all, we select the ten most intense geomagnetic storms of the last two decades, going further back in time would have meant a lower amount of available geomagnetic data. These storms are listed in Table 1, ordered by decreasing intensity based on the minimum value reached by *Sym-H* index [King & Papitashvili, 2005]. Then we look for a set of magnetic observatories, approximately uniformly spaced in geomagnetic latitude, with data available for some of the storms listed in Table 1. The optimal configuration came out to be a set of 25 observatories that, with a few exceptions, had data available for six out of the ten selected storms. Some details on these observatories are listed in Table 2 and their position, in a geomagnetic coordinates grid, is shown in Figure 1 by green circles. *Sym-H* index [Iyemori, 1990] corresponding to the selected storms is shown in Figure 2 for the four days characterised by the most intense geomagnetic activity, over which the analysis has been performed. Two of these storms, i.e. those of October 2003 and November 2004, are actually a double and a triple dip storm, respectively [Farrugia et al., 2006]. As mentioned above, data from the selected magnetic observatories are not available for all the selected storms. One case is that of March 1989 geomagnetic storm, the furthermost among those chosen, for which data

from BEL, SJG, KOU, PHU, GUA, BNG, HUA, ASC, PAF magnetic observatories (most unfortunately covering equatorial latitudes) are not available. The decision to keep this storm anyway derives from the exceptional low value of -720 nT reached by *Sym-H* index. Other missing data are those from GUA (July 2000 storm), ASC (March 2001 storm), BNG (November 2003 storm) and HBK (November 2004 storm). Looking at Table 2 it emerges that the uniformity of spacing in geomagnetic latitude is broken at the equator, where the density of observatories is higher. This stems from the will to well document what happens at equatorial latitudes and from the need to replace GUA with BNG for July 2000 storm and ASC with HUA for March 2001 storm. Certainly, we could have used all the observatories available for each geomagnetic storm but we preferred to deal always with the same set of samples to better compare the results. Moreover, considering that this set consists of observatories with sparse longitudes, and magnetic local time (MLT) of recorded *GIC* index maxima are not taken into account, a different set of observatories for each storm would have complicated interpretation of results consistently. Since the results may be biased from storm to storm in terms of an absolute value of *GIC* index due to the different geomagnetic longitudes, we display the same analysis performed on the set of 25 magnetic observatory also for a set of 14 observatories. These have geomagnetic longitudes between about 7° W and 38° E (grey area of Figure 1), namely on a band of around 45 degrees equivalent to a difference of 3 hours in MLT; details are listed in Table 3. The limited number of observatories selected in this case is a direct consequence of magnetic observatories geographical distribution and data availability. Of course if, on one side, such a loose chain of observatories does not allow a well-resolved investigation of the latitudinal dependence of GIC intensity, on the other side, it allows better discriminating ionospheric and magnetospheric currents effects based on the MLT position of the observatory. However, even if it were possible to build dense latitudinal chains, the limit to the accurate observation of the latitudinal variation of GIC intensity maxima would be the rapid variability of ionospheric current systems. For example, the dayside EEJ has a relatively short (2.4 hour) correlation length in longitude [Alken & Maus, 2007], so the largest signature of the EEJ could be missed by the observatories for any given storm.

Table 1: The ten largest (based on the minimum value reached *Sym-H* index) geomagnetic storms of the last 20 years, ordered by decreasing intensity. The time of SSC is also indicated as reference for the beginning of the storm. Asterisks indicate the storms selected for this study.

Date of SSC	**Time of SSC (UT)**	***Sym-H*$_{min}$ [nT]**
13 March 1989*	01:27	-720
20 November 2003*	08:02	-490
29 October 2003*	05:50	-490

31 March 2001*	00:52	-437
13 July 1982	16:18	-436
7 November 2004*	10:52	-394
6 February 1986	13:12	-379
15 July 2000*	14:37	-347
11 April 1981	13:39	-343
24 March 1991	03:41	-337

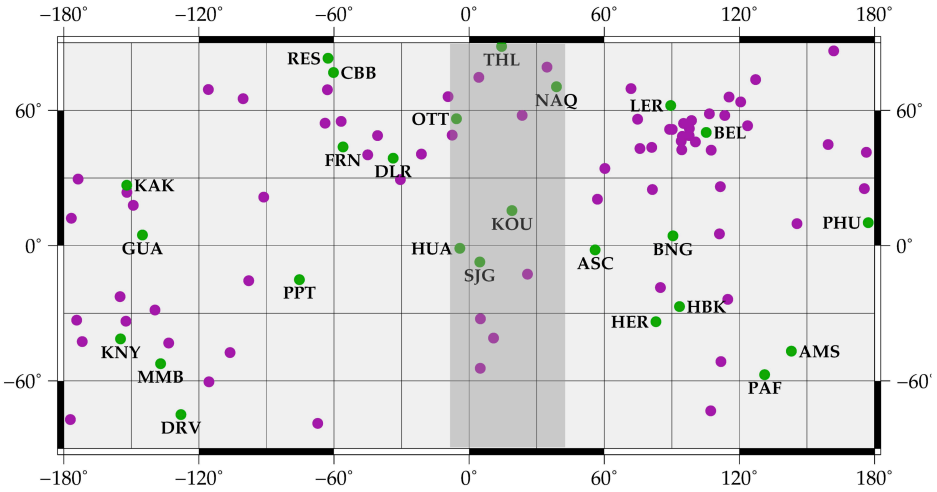

Figure 1: Distribution of selected magnetic observatories in the geomagnetic reference frame. IAGA codes are reported only for the set of 25 magnetic observatories used in the first part of the investigation (green circles). The grey area identifies the longitude band where the set of 14 magnetic observatories is located. For the additional 79 magnetic observatories used in the last part of the investigation, only the position is indicated (purple circles).

Table 2: Geomagnetic latitudes and longitudes of the set of 25 magnetic observatories ordered by increasing geomagnetic latitude; the last column indicates the number of hours to add to UT 00:00 to obtain MLT location of each observatory.

IAGA Code	Observatory Name	Geomagnetic latitude °N	Geomagnetic longitude °E	Difference in hours between UT 0 and MLT
DRV	Dumont d'Urville	-74.96	-127.96	-13
PAF	Port-aux-Francais	-57.26	131.21	+4
AMS	Martin de Vivies	-46.83	143.08	+5
HER	Hermanus	-33.78	82.93	+1
HBK	Hartebeesthoek	-27.04	93.39	+1
PPT	Pamatai (Papeete)	-15.10	-75.36	-10
ASC	Ascension Island	-1.90	55.93	-1
HUA	Huancayo	-1.19	-4.15	-5
BNG	Bangui	4.32	90.49	+1
GUA	Guam	4.70	-145.06	-14
PHU	Phuthuy	10.16	177.19	+7
KOU	Kourou	15.53	19.00	-3
KNY	Kanoya	21.25	-159.97	-15
KAK	Kakioka	26.76	-152.03	-15
SJG	San Juan	28.95	5.37	-4
MMB	Memambetsu	34.75	-149.58	-15
DLR	Del Rio	38.76	-33.73	-7
FRN	Fresno	43.77	-56.00	-8
BEL	Belsk	50.20	105.26	+2
OTT	Ottawa	56.25	-5.64	-5
LER	Lerwick	62.12	89.49	+1
NAQ	Narsarsuaq	70.45	38.75	-3

CBB	Cambridge Bay	76.75	-60.22	-10
RES	Resolute Bay	83.11	-62.68	-10
THL	Qaanaaq (Thule)	88.32	13.88	-5

As already mentioned in the Introduction, a further part of the investigation relies on a much wider set of 104 magnetic observatories, for the study of the November 2004 storm only. The additional 79 observatories are shown in Figure 2 as purple circles. Apart from CBI, CTS, DOB, ELT, HTY, KIR, LRV and LVV they are all observatories participating to the INTERMAGNET program, hence with a guaranteed quality of the measurements.

For all the selected observatories, we considered the X and Y Cartesian components when directly available, or differently calculated them from the horizontal component and declination. Gaps have been linearly interpolated if not occurring during time intervals characterised by the most intense and rapid variations, otherwise the observatory has been excluded for the storm under evaluation. As explained in more detail in the next section, linear interpolation used for gap filling is not expected to change excessively *GIC* index estimation as far as to alter results.

Table 3: Geomagnetic latitudes and longitudes of the set of 14 magnetic observatories ordered by increasing geomagnetic latitude; the last column indicates the number of hours to add to UT 00:00 to obtain MLT location of each observatory.

IAGA Code	Observatory Name	Geomagnetic latitude °N	Geomagnetic longitude °E	Difference in hours between UT 0 and MLT
AIA	Argentine Islands	-54.42	4.92	-4
PST	Port Stanley	-41.05	10.82	-4
TRW	Trelew	-32.46	4.99	-4
VSS	Vassouras	-12.66	25.89	-3
HUA	Huancayo	-1.19	-4.15	-5
KOU	Kourou	15.53	19.00	-3
SJG	San Juan	28.95	5.37	-4
FRD	Fredericksburg	49.01	-7.53	-5
OTT	Ottawa	56.25	-5.64	-5
STJ	St John's	57.78	23.54	-3
NAQ	Narsarsuaq	70.45	38.60	-2
IQA	Iqaluit	74.62	4.29	-4

GDH	Godhavn	79.15	34.58	-2
THL	Qaanaaq (Thule)	88.31	13.88	-4

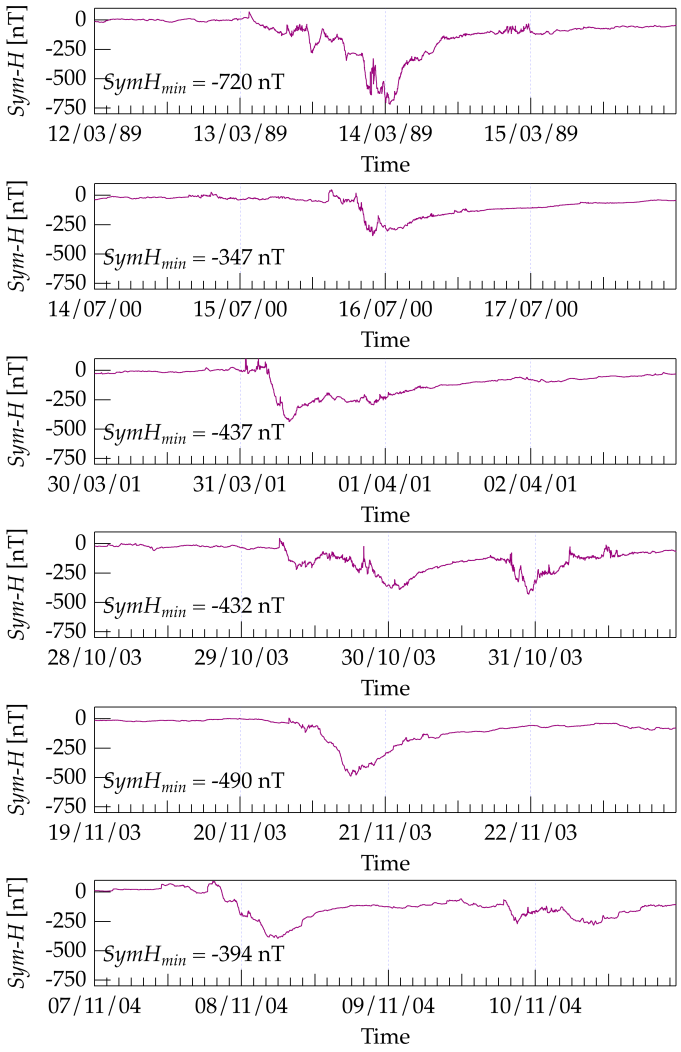

Figure 2: *Sym-H* index of the selected geomagnetic storms, ordered from the furthermost to the most recent.

III. ESTIMATION OF *GIC* INDEX

Measurements of GIC intensity are generally made along electric power grids or along pipelines. These, however, are not easily retrievable and do not cover the entire globe. Another way to study GIC is through the geoelectric field induced at the Earth's surface. This can be done both in the time and in the frequency domains [Pirjola, 2002] by assuming a model for Earth's conductivity that, in the best case, is a uniformly conducting half-space

and, in the worst, considers an anisotropic conductivity. The latter requires the introduction of tensors, hence ending in the estimation of reasonably complicated formulas. For this reason, several proxies of the geoelectric field, and consequently of GIC intensity, have been investigated in the years. Of course, resorting to proxies means neglecting very important factors that determine GIC intensity, as the technical specifications of the power grid and ground conductivity. There are several proxies based on geomagnetic data (e.g. the time derivative of the geomagnetic field $\mathrm{d}B/\mathrm{d}t$, A and K indices, hourly standard deviation of X and Y components, etc.) that can be used as indicative of GIC intensity. All of them somehow represent the way the geomagnetic field varies in time since, as broadly established, the origin of GIC is to be searched in the time rate of geomagnetic field variations [Thomson et al., 2010]. Recently, while looking for spectral information on the relationship between the pipe-to-soil potential (PSP) and variations in the horizontal components of the geomagnetic field, Marshall et al. [2010, 2011] developed a new index, i.e. the *GIC* index, characterised by a 1-minute sampling rate. For this reason, proxies providing the poorest information on GIC evolution are certainly A and K indices being characterised by a sampling rate of three hours. Differently, hourly standard deviation provides results comparable to those obtained with the *GIC* index but with a lower time resolution, of one hour instead of one minute. The comparison between the performance of some of the above cited proxies, in particular of $\mathrm{d}B/\mathrm{d}t$, with that of *GIC* index in the representation of actual measurements of the PSP has shown that this index is the one that best agrees (based on correlation analysis) with real measurements. Values of the correlation coefficient between PSP and *GIC* index resulted to be higher than those between PSP and $\mathrm{d}B/\mathrm{d}t$ of at least 0.3-0.4, generally superseding values of correlation coefficient of 0.8. So far, the performance of this index has been tested only at the geomagnetic latitudes of Australia and New Zealand [e.g. Alekseev et al., 2015], i.e. approximately between 20°S and 50°S, therefore its validity at latitudes outside this range cannot be taken for granted due to the role of local conductivity on GIC intensity. However, due to the not uniform conductivity of Australia and New Zealand themselves we assume that *GIC* index works well independently of conductivity also outside the 20°S - 50°S geomagnetic latitude range.

GIC index can be straightforwardly computed from 1-minute values of the X and Y Cartesian components of the geomagnetic field measured at a given observatory according to the following equation:

$$\begin{aligned} GIC_x(t) &= \left| FFT\left\{ Y(f)\cdot Z(f) \right\}^{-1} \right| \\ GIC_y(t) &= \left| FFT\left\{ X(f)\cdot Z(f) \right\}^{-1} \right| \end{aligned} \tag{1}$$

with $Z(f)$ a filter function defined as

$$Z(f) = \sqrt{\frac{f}{f_N}} \cdot e^{i\cdot\frac{\pi}{4}} \tag{2}$$

where f is a variable frequency, f_N=8.3~mHz is the Nyquist frequency for data sampled at a rate of one value per minute, $FTT\{\}^{-1}$ indicates the inverse Fourier transform and $||$ the absolute value. More details on this index can be found in Marshall et al. [2010, 2011, 2012]. Considering the large amount of available geomagnetic data, this index proves to be a powerful tool to perform investigations concerning GIC over large spatial scales or wherever real GIC measurements are not available. These are the reasons why we relied on *GIC* index.

All estimates of GIC_x and GIC_y indices shown by Marshall et al. [2011] are performed on a single-day of observations (1440 points); before calculating the FFT, the time series are multiplied by a Hanning function in the time domain with the purpose to limit end effects. Here, however, we deal with time series with a length of four days (5600 data points) and the use of the procedure above inevitably produces a 1-day modulation of GIC_x and GIC_y indices, due to the shape of the Hanning function. This function has the disadvantage to excessively damp *GIC* indices at the borders of the considered time window. For this reason we used a slightly different procedure to calculate GIC indices. First, we removed from the *X* and *Y* components their averages estimated over the entire 4-day interval. Then, we considered windows of 1440 points and, to limit end effects and avoid the 1-day modulation, used a moving window approach. In practice, we followed these steps: a) estimate equations 1 and 2, b) record their maximum value at the centre of the window, c) shift the window of 1 point (i.e. 1 minute) and repeat the procedure. Some tests have been performed to evaluate the sensitivity of *GIC* indices to the width of the window used for FFT estimation. Comparison of *GIC* indices obtained using different widths of the FFT window (1, 3, 6, 12 and 24 hours) has shown their very low sensitivity to the window's width (results not shown).

Based on the way *GIC* index is defined, it follows that the linear trends used to fill data gaps, when existing, are not expected to amplify it but, in case, to underestimate it. In fact, *GIC* index takes high values where high rates of change in the geomagnetic field are present; this is not the case of intervals covered by a linear trend. Moreover, we recall that when gaps occurred during time intervals characterised by rapid and wide variations of the geomagnetic field (i.e. corresponding to highly disturbed geomagnetic conditions), data from that observatory have been discarded. Ultimately, the underestimation of *GIC* index due to gap filling is done exclusively during phases of the storm where the index would not have reached its highest values anyway and, as illustrated in what follows, only *GIC* index maximum values are considered in the analysis.

Figure 3 shows an example of *GIC* index estimation obtained for the *X* and *Y* components measured at three observatories at different geomagnetic latitudes (high, middle and low).

Figure 3 anticipates some results concerning the intensity of GIC at equatorial latitudes that will be discussed in the next section. Here, we just would draw attention to how amplitudes of GIC_y index vary from CBB (high latitude) to HUA (equatorial latitude). We also observe that, being estimated on the X component, GIC_y is expected to be generally larger than GIC_x because of the different contributions of magnetospheric and ionospheric currents on the two components. Current systems responsible for the strongest external contributions of the geomagnetic field (e.g. ring current, auroral and equatorial electrojets) exert their action mainly on the meridional plane, thus affecting X component more than Y component.

The analysis shown in Figure 3 for CBB, FRN and GUA is performed on both X and Y components measured at the two sets of 25 and 14 observatories, for the selected geomagnetic storms. The same analysis is also performed on the extended set of 104 observatories only for the November 2004 geomagnetic storm. Obtained results are displayed and discussed in the next section.

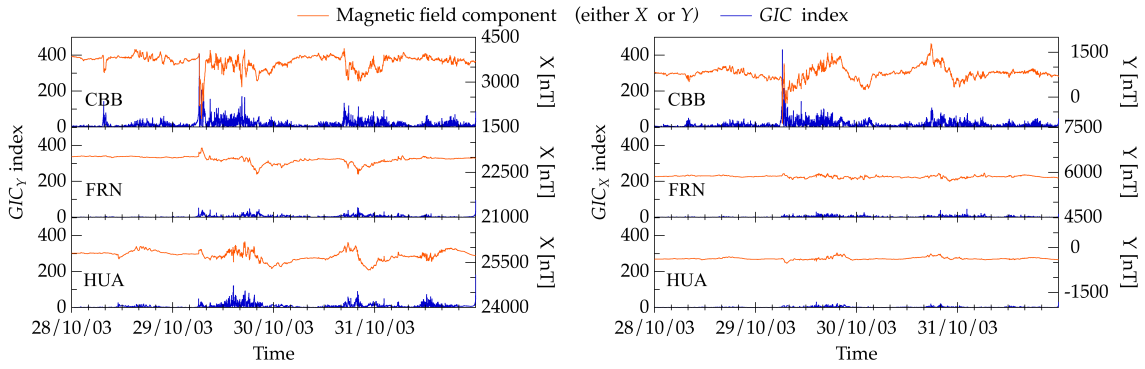

Figure 3: X and Y components (orange), GIC_x and GIC_y indices (blue) for three observatories at different geomagnetic latitudes (CBB: 76.75°N; FRN 43.77°N; HUA: -1.19°N) during the Halloween geomagnetic storm (28-30 October 2003).

IV. Results and Discussion

To obtain the latitudinal profile representing GIC maximum intensity, for each geomagnetic storm, we estimate GIC_x and GIC_y indices from data of the selected observatories, and then record their maximum values over the 4-day time interval shown in Figure 2. This procedure is applied following two different approaches: 1) regardless of considerations on the magnetic local time of the observatory (set of 25 magnetic observatories) to indirectly measure, through *GIC* index, the peak of GIC intensity throughout the geomagnetic storm; 2) focusing on a restricted MLT interval (set of 14 magnetic observatories) to obtain a latitudinal profile of *GIC* indices maximum values less biased from storm to storm. Results corresponding to the set of 25 magnetic observatories are shown in Figure 4 where the single

point represents the maximum *GIC* index estimated at given magnetic observatory during a given geomagnetic storm and the different colours represent the different storms. In this phase of the study, the double and triple dip storms of October 2003 and November 2004, respectively, are treated as a single storm. The following main features are recognisable in Figure 4: from the polar cap *GIC* indices increase and reach their peak values at auroral oval latitudes, then they gradually decrease moving toward middle and equatorial latitudes where, in some cases, we observe an increase.

The dependence of *GIC* indices with latitude depend is determined by the location and dynamics of the sources inducing the geoelectric fields. The values found at polar cap latitudes, smaller than those observed at auroral oval latitudes, can be explained in terms of the lower intensity of the currents flowing there, that is a consequence of the low conductive polar cap ionosphere [Mc Granaghan et al., 2016]. Moving equatorward, *GIC* indices take the highest value over the auroral oval due to the intensification of the auroral electrojects and of the field aligned currents; under heavily geomagnetically disturbed conditions they are both characterised by rapid and wide time variations causing analogous variations in the geomagnetic field. Getting far from the auroral oval, a sharp decrease of *GIC* indices is observed at geomagnetic latitudes of around 50°. These latitudes are less affected by the polar ionospheric currents and other sources, as for instance the ring current, could play a dominant role. However, the ring current is very far from the Earth's surface and, consequently, its contribution to geomagnetic field variations is about one order of magnitude less than that of polar ionospheric currents.

Finally, Figure 4 evidences an increase of *GIC* indices at equatorial latitudes, also reported by other authors [Pulkkinen et al., 2012; Nwgira et al., 2013; Carter et al. 2015, 2016; de Villiers et al., 2017; Moldwin et al., 2016]. At these latitudes, the EEJ flows in the E-region of the dayside ionosphere (altitudes of around 100 kilometres). This narrow ribbon of current closely follows the geomagnetic equator and corresponds to an eastward electric current. Looking at GIC_x index the increase is detectable in BNG during the November 2004 geomagnetic storm, the peak occurring at around 00:00 UT on the 9 of November corresponding to an MLT of around 01:30, which makes it difficult to justify an interpretation in terms of an increase of the EEJ that flows on the dayside. Moreover, since EEJ flows on the equatorial plane, its effect is expected to be visible in the *X* component of the geomagnetic field and not in the *Y* component, used to estimate GIC_x index. Concerning GIC_y index, the increase is detectable in HUA during the geomagnetic storms occurred in: October 2003, November 2003 and November 2004. These peaks are, respectively, at around: 20:00 UT on 30 October 2003 corresponding to an MLT of around 15:00; 18:30 UT on 7 November 2003 corresponding to an MLT of around 15:00; 13:00 UT on 20 November 2004 corresponding to an MLT of around 08:00. Due to their MLTs, the first two enhancements are well compatible with an increase of GIC_y index deriving from an increase of the EEJ that on turn influenced the *X* component. Although less clear, also the third case can be a consequence of EEJ enhancement, indeed at 8:00 MLT its intensity is certainly lower than that corresponding to

12:00 but it is anyway not negligible. In fact, the maximum value of GIC_y index is smaller than those observed in the other two cases. The reason why this enhancement is not observed during March 2001 geomagnetic storm relates to fact that the maximum value of GIC_y index is reached at 22:00 MLT at HUA, during times when the EEJ is not present overhead. Concerning July 2000 geomagnetic storm, GIC_y index maximum is reached at 17:00 MLT, a time when a weak EEJ is still present. In this case, however, the low intensity of the July 2000 geomagnetic storm could have prevented equatorial electrojet from being affected by intense variations and therefore GIC_y index from reaching values higher than those observed under less disturbed conditions.

At EEJ latitudes, however, also the counter electrojet (CEJ) can be observed, particularly in the early morning and evening. When CEJ occurs, the daytime EEJ strength is weakened and reverses direction for a short period. It has also been found that EEJ and its CEJ are characterised by a marked longitudinal variability [Rabiu et al., 2017]. This makes the source, i.e. either the EEJ or CEJ, of the equatorial enhancement of maximum *GIC* indices not obvious. Rabiu et al. [2017] found that CEJ has the greatest % of occurrence in the African stations and that, among the observatories they considered, HUA is the one characterised by the strongest EEJ and the least occurrence of the CEJ. Therefore, the enhancement of maximum *GIC* indices we find at HUA can be quite safely ascribed to the EEJ.

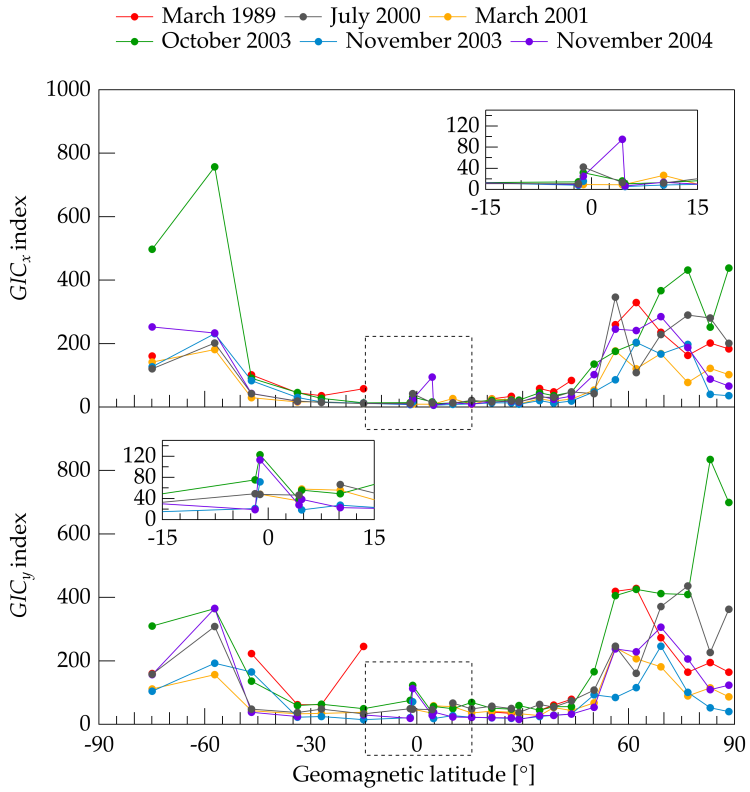

Figure 4: Coloured traces indicate the maximum *GIC* index (top: GIC_x index; bottom: GIC_y index) estimated at the 25 selected magnetic observatories during the six selected geomagnetic storms. Inset figures represent an enlarged view of the plots around equatorial latitudes (from -15° to 15° of geomagnetic latitude).

Averaging over the six storms the trends plotted in Figure 4, we obtain the latitudinal profiles of *GIC* indices shown in Figure 5 (purple dotted lines) with associated error bands estimated, for each observatory, as the standard deviation of the six samples. The green line in Figure 5 represents a smoothed and spline-interpolated version of the average. This Figure shows that a ramp begins at geomagnetic latitudes of about -45° and 45°, meaning a high rate of increase of the maximum values of *GIC* indices and hence an augmented risk of damages due to the building up of geomagnetically induced currents. The latitude threshold boundary found by our analysis seems to be at about 45°- 50° of geomagnetic latitude. The two trends obtained from GIC_x and GIC_y indices are very similar, nevertheless small differences can be observed. Both trends are characterised by different profiles for the Southern and Northern high latitudes. This is probably due to the better sampling of high Northern latitudes than Southern ones, even if it cannot be excluded that the asymmetries between the two polar regions provide an effect. GIC_y index profile presents a sort of bump (i.e. the effect of the equatorial electrojet on the *X* component), not present in GIC_x index. However, the general trends obtained (i.e. peak at high-latitudes, dip in mid-latitudes and a smaller peak at EEJ zone) are consistent with the profiles reported, for instance, by Pulkkinen et al. [2012] and Ngwira et al. [2013]. Pulkkinen et al. [2012], considering only the two extreme storms of March 1989 and October 2003, found a sudden drop in all the parameters they investigated as geoelectric field proxies, between 40° and 60° of geomagnetic latitude and an increase at equatorial geomagnetic latitudes between -5° and 5°. Interestingly, Pulkkinen et al. [2012] observed also a general tendency to have a slightly larger amplitude for all the analysed parameters in the Northern Hemisphere than in the Southern one. Ngwira et al. [2013] considered 12 severe/extreme geomagnetic storms and used, as a proxy of the geoelectric field, dB/dt. They found the latitude threshold boundary at about 50°-55° of geomagnetic latitude and attributed this boundary to the movement of the auroral oval. Ngwira et al. [2013] found also that the ground induced geoelectric field at the latitudes of the EEJ can be one order of magnitude larger than outside the EEJ belt and that this enhancement is the consequence of the penetration of high latitudes electric field. Concerning North-South asymmetries, their Figure 2 shows a slight difference between the two hemispheres. The capability to capture features of the latitudinal profile of GIC intensity found by other authors strengthens the use of *GIC* index also outside the geomagnetic latitudinal range of Australia and New Zealand.

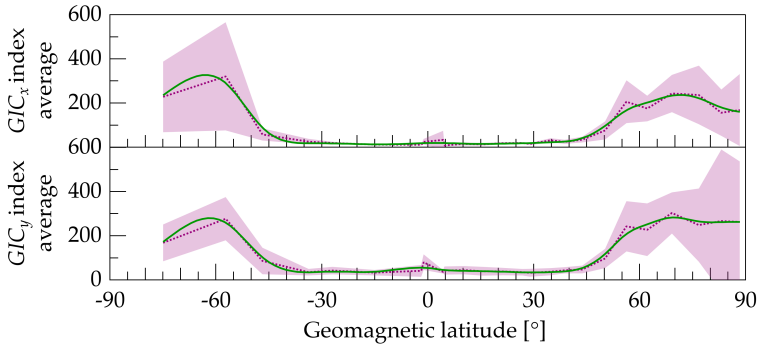

Figure 5: Purple dotted line indicates the *GIC* index (top: *GICx* index; bottom: *GICy* index) averaged over the six selected geomagnetic storms. Shadowed areas indicate the error band represented by the standard deviations at each observatory. Green line indicates a smoothed version of the average trend.

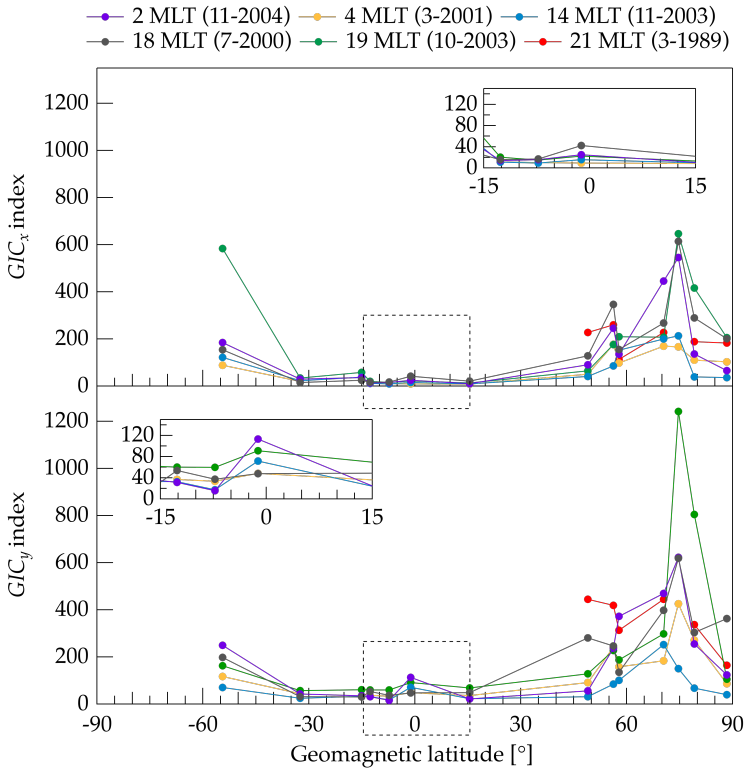

Figure 6: Coloured traces indicate the maximum *GIC* index (top: GIC_x index; bottom: GIC_y index) estimated at the set of 14 selected magnetic observatories during the six selected geomagnetic storms. Inset figures represent an enlarged view of the plots around equatorial latitudes (from -15° to 15° of geomagnetic latitude). MLT corresponds to the UT of *Sym-H* absolute minimum.

Figure 6 is the same as Figure 4 but obtained considering the set of 14 observatories with longitudes within a band of 45 degrees and MLTs within three hours. The top of Figure 6 reports the value of MLT corresponding to the UT of *Sym-H* absolute minimum over the 4-day interval. Concerning the latitudinal profile of the maximum intensity of GIC, main features are similar to those shown in Figures 4 and 5, but Figure 6 contains additional information with respect, for instance, to the current systems responsible for the observed enhancement of *GIC* indices. At high Northern latitudes, two peaks are clearly visible in the GIC_x index at 55° and 75° of geomagnetic latitude. These latitudes are compatible with the position, during disturbed conditions, of field-aligned currents [Green et al., 2009] that generate the most visible signature in the *Y* component. *GIC* indices enhancement at middle and high latitudes reaches the lowest values when the observatories are in the dayside at the moment of the main phase of the storm. This does not hold for equatorial latitudes where the increase of GIC_y index is observed almost independently of MLT. These features can be explained in terms of the asymmetries of ionospheric and magnetospheric current systems that, with the exception of the EEJ, are generally more intense in the nightside. This kind of approach demonstrates the importance of considering the MLT position of the observatory in the reconstruction of latitude profiles since information that could be useful for GIC related risk protection is provided. Unfortunately, this kind of study is seriously limited by the availability of observations.

So far, we have ignored the fact that two of the storm events here considered are actually a double and triple dip storm. Figure 7a shows separately *GIC* indices latitudinal behaviours for the double dip storm of 7 November 2004 estimated from the *X* and *Y* magnetic measurements of 104 ground stations, regardless of MLT. To split this double storm in two, the time interval of four days is divided in two periods of 2880 points each. Despite the first storm is more intense in terms of *Sym-H* index (see Figure 2) than the second, from Figure 7a it seems that noticeable differences between the two storms are observed only at high latitudes, with effects stronger during the second storm due to the intense electric currents flowing in the polar regions (as can be deduced by *AE* index reported in Figure 7b). Looking more carefully at what obtained for the Northern polar latitudes for the second storm, we could interpret the different shape of the profiles of GIC_x and GIC_y indices in terms of their different sources. The profile of GIC_x index around 70° is clearly sharper than that of GIC_y index and the double peak visible in Figure 6 where MLT is considered, is no more visible. Recalling that GIC_x index is estimated from the *Y* component, which is affected mainly by electric currents perpendicular to its direction, we could interpret the reduced band of latitudes where the highest values of GIC_x index are observed in terms of the Pedersen currents that cover a small latitudinal band. They flow along meridional planes between the footprints of the region 1 and region 2 field-aligned currents [Prölls, 2004]. Similarly, recalling that GIC_y index is estimated from *X* component we can deduce that the increased band of latitudes where the highest values of GIC_y index are observed is that corresponding to the flow of auroral electrojects. The fact that this distinction is not evident

during the first storm (right side of Figure 7a) can be due to the less intense auroral activity during the period between 7 November, 00:00 and 8 November, 23:59 as can be verified in Figure 7b displaying *AE* index. We also observe that the average smoothed trend obtained considering 25 observatories and six geomagnetic storms well agrees with the trend reconstructed with the 79 additional magnetic observatories and for a single storm. Certainly, further analyses are needed to univocally interpret the latitudinal profile of GIC index in terms of ionospheric current systems.

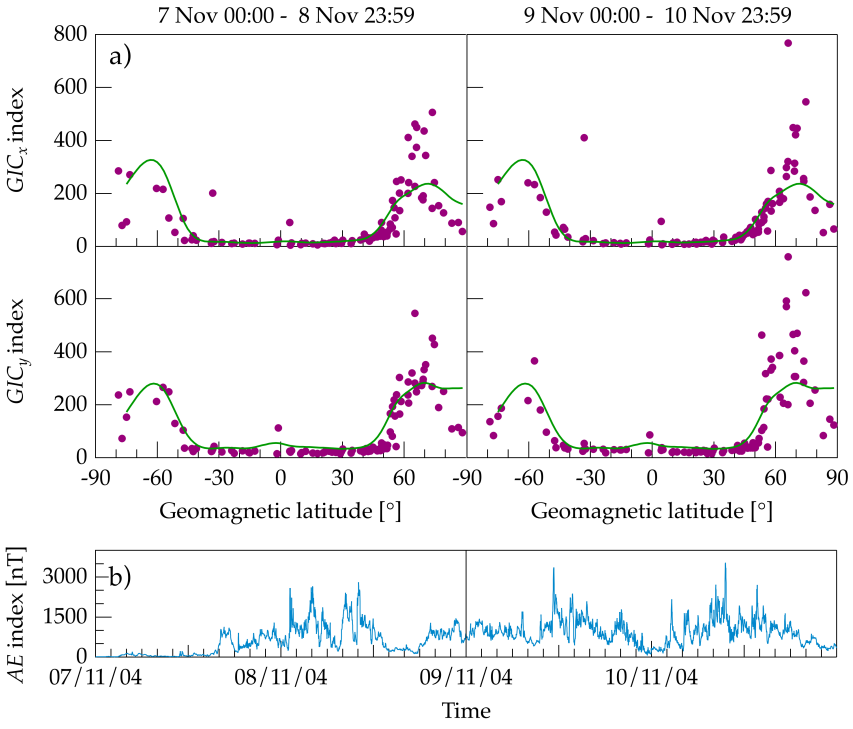

Figure 7: a) Purple circles indicate the *GIC* index (top: *GICx* index; bottom: *GICy* index) maximum values for the November 2004 double-geomagnetic storm separately for the two storms. Overlaid green line indicates a smoothed version of the average (over the six storms) trend. b) *AE* index during the November 2004 geomagnetic storm.

As a last analysis, we considered the time interval between 16:00 UT of 7 November 2004 and 22:00 UT of 8 November 2004, and instead of taking the maximum values of *GIC* indices over the entire 4-day time interval, we took the maximum values over successive intervals of two hours. This is equivalent to follow the evolution of *GIC* indices latitudinal profile with a time sampling of two hours. Results are displayed in Figures 8 and 9 for GIC_x and GIC_y indices, respectively. Moving from top to bottom each blue-circle trace represents the *GIC* indices latitudinal profile sampled at a time rate of 2 hours starting from 7 November 2004, 14:00 to 8 November 2004, 20:00 UT. For example, the latitudinal profile shown in

the first row is estimated taking the maximum value of *GIC* indices, al all magnetic observatories, in the time interval 7 November 2004 14:00 - 7 November 2004 15:59. The successive profile is estimated considering the successive 2-hour interval. Figures 8 and 9 show also *AE* index and *Sym-H* index in order to recognise the phases of the geomagnetic storm and associate them with the different shapes of *GIC* indices latitudinal profiles.

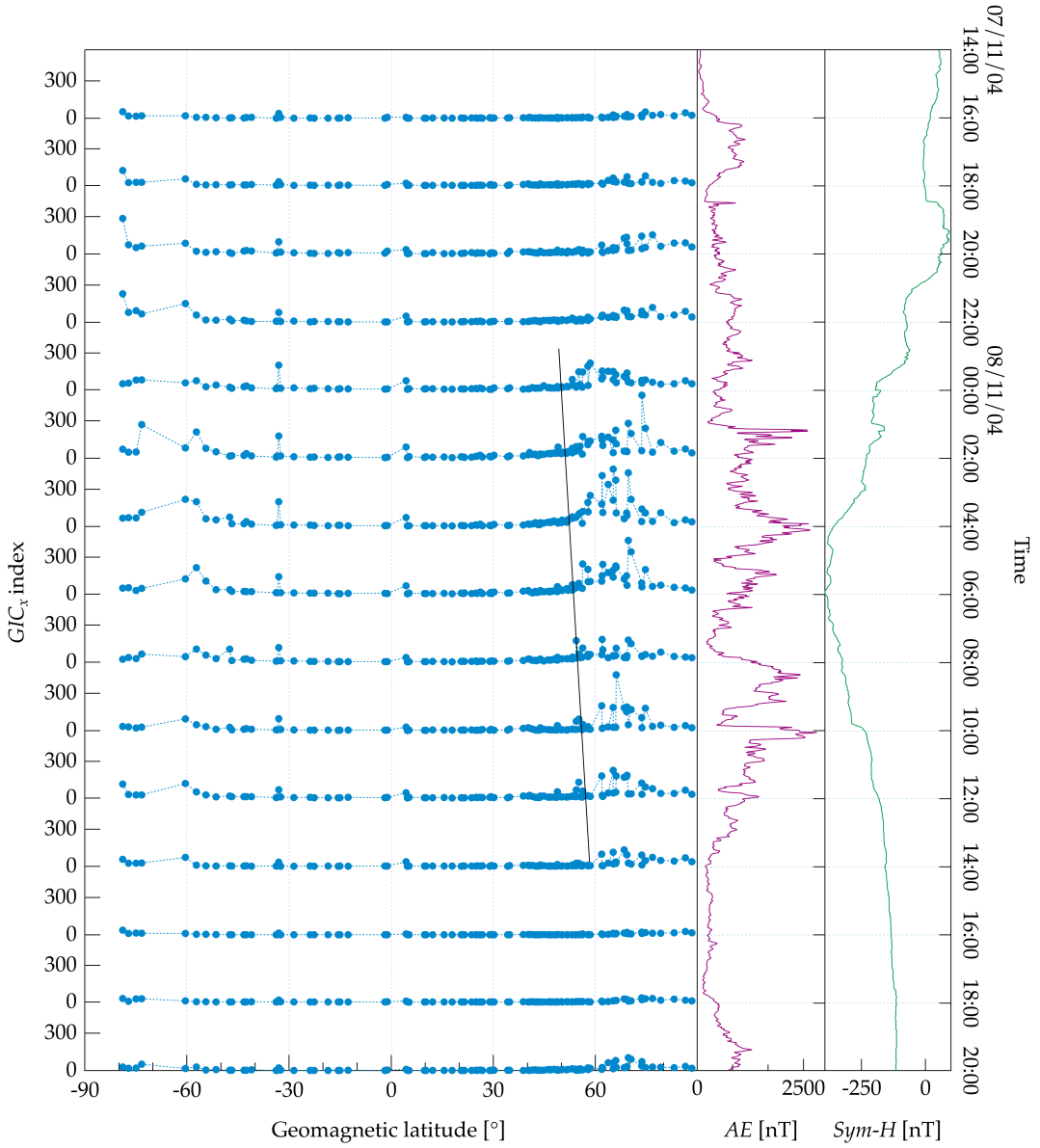

Figure 8: On the left: maximum values of *GICx* index estimated over 2-hour time intervals from 7 November 2004, 14:00 UT to 8 November 2004, 20:00 UT (time flowing from top to bottom). On the right: *AE* and *Sym-H* indices over the same time interval. Black line indicates the time-varying position of the southernmost boundary of the band of latitudes most affected by high values of *GIC* index during the different phases of the storm.

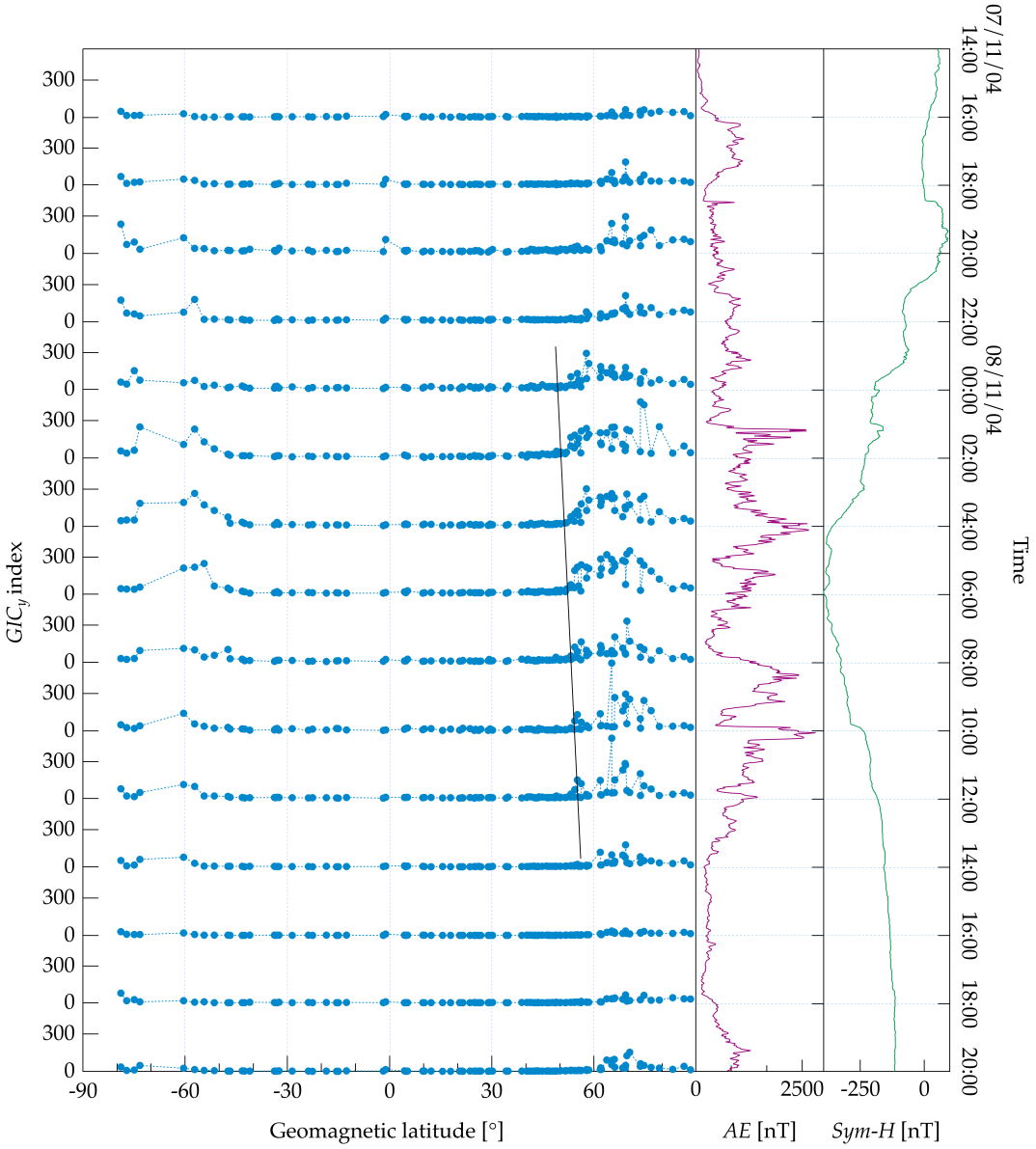

Figure 9: On the left: maximum values of *GICy* index estimated over 2-hour time intervals from 7 November 2004, 14:00 UT to 8 November 2004, 20:00 UT (time flowing from top to bottom). On the right: *AE* and *Sym-H* indices over the same time interval. Black line indicates the time-varying position of the southernmost boundary of the band of latitudes most affected by high values of *GIC* index during the different phases of the storm.

Focussing on the Northern Hemisphere where the *GIC* indices latitudinal profiles are reconstructed with a higher resolution than in the Southern Hemisphere, Figures 8 and 9 show that the profiles at the high latitudes well match with the evolution of the geomagnetically disturbed conditions, represented by *Sym-H* and *AE* indices. For instance, in the time interval 18-20 UT it is possible to recognise a sudden increase in *Sym-H* index that produces, in the same time interval, an increase of *GIC* indices maxima well visible at high

latitudes. Starting from 22 UT we observe a gradual decrease of *Sym-H* index, corresponding to an intensification of the ring current, and an increase of *AE* index corresponding to an intensification of the auroral currents. With the start of auroral activity, the latitudinal profile grows at latitudes corresponding to those of the auroral oval, showing a widening of the band of latitudes most affected by high values of *GIC* index together with an equatorward shift of the southernmost boundary of this latitude band. Then, as time passes, the band of disturbed latitudes reduces and moves back to its original position. We suppose that this band of latitudes could be representative of the latitudes covered by the auroral electrojets. The black line displayed in Figure 8 and 9 seems to be indicative, in this case, of the equatorward boundary of the auroral oval. This behaviour leads us to speculate that such a use of *GIC* index could be viewed as a tool to nearly real-time monitor the displacement of the auroral oval during geomagnetically perturbed conditions and hence of the latitude threshold boundary. Certainly, the technical feasibility of this idea needs a thorough and dedicated investigation that is not the purpose of this paper. Once cleared the technical limitations its achievement would depend, anyway, on the availability of real time 1-minute data from magnetic observatories.

To conclude, it is worth spending a few words on two features of Figures 8 and 9. One concerns equatorial latitudes. In Figure 8 a signature that could be ascribed to the EEJ is visible both at the commencement and in the main phase of the storm, while in Figure 9 an enhancement of the maximum GIC_y index is seen only at the storm commencement. This can be explained in terms of the different MLT position of the two observatories involved, i.e. BNG and HUA. In Figure 8 the enhancement is seen at BNG that, at 18 UT, was at 19:30 MLT. This enhancement cannot be ascribed to the EEJ due to the MLTs covered by BNG during the storm (i.e. corresponding to evening and early morning) and also to the fact that it is observed in GIC_x index (i.e. to the *Y* component). Differently, the enhancement visible in Figure 9 in GIC_y index, and hence in the X component of the geomagnetic field, correctly relates to the EEJ since HUA observatory was at around 13-15 MLT during the storm commencement (between 18-20 UT). During the same interval GIC_x index, and hence in the *Y* component of the geomagnetic field, does not show an appreciable increase. The second feature concerns the unexpected peaks visible in Figure 8, practically at all UTs, around -30° of geomagnetic latitude and that we are not able to explain. These data correspond to the observatory of Learmonth (IAGA code: LRM), they have been double-checked but we found no reason to discard them. At 18 UT, LRM was at 1:30 MLT so the observed peak at the commencement and in the main phase corresponds to MLTs in the night and morning sectors.

V. CONCLUSIONS

The purpose of this study is the investigation of the impact of geomagnetically induced currents with latitude. Although similar researches have been performed in the past [e.g. Pulk-

kinen et al., 2012; Ngwira et al., 2013], here we propose an analysis based on a different proxy of the geoelectric field. Instead of using dB/dt, we estimated the *GIC* index [Marshall et al., 2010, 2011] that has proved to correlate with actual measurement of the pipe-to-soil potential better than dB/dt at geomagnetic latitudes between 20°S-50°S. We reconstructed a latitudinal profile of maximum *GIC* indices values using two sets of magnetic observatories, with different geographical distribution, for six geomagnetic storms. Then we went more in depth using a larger set of magnetic observatories (104) and investigated what happened during a single geomagnetic storm, that of 7 November 2004. For such storm, we investigated also the time variations of the latitudinal profile with a sampling rate of 2 hours. Findings can be summarised as follows:

1) The enhancement of the EEJ is recognisable in GIC_y index; even though values are low it can anyway pose a risk of GIC damages to countries passing across an MLT from 8:00 to 18:00 during a geomagnetic storm;

2) The latitudinal profile of GIC intensity does not vary sensibly from storm to storm and the latitude threshold boundary can be set at about 45°-50° of geomagnetic latitude;

3) Through *GIC* index latitudinal profile it could be possible to distinguish the sources producing definite features;

4) Through the middle and high latitude portion of *GIC* index latitudinal profile it could be possible to monitor the displacement of the auroral oval during geomagnetically disturbed conditions;

5) Results support the use of *GIC* index at all latitudes.

An accurate definition of the way maximum GIC intensity varies with latitude plays an important role especially at low and middle latitudes that are generally, and erroneously, considered safe from damages related to space weather events. Concerning middle latitudes, although it is true that the bulk of effects are produced by the magnetopause currents there, it should not be neglected that the auroral can expand equatorward consistently as, for instance, happened during the 28-30 October 2003 geomagnetic storm [Thomson et al., 2010].

According to Marshall et al. [2012], the next phase of this study could be to examine separately events dominated by the dynamics of the auroral currents or by that of the magnetopause currents. Indeed, it has been found that the decrease of the maximum value of dB/dt from high to middle latitudes depends on the type of event considered, either geomagnetic storms or sudden impulses events. To conclude, we underline that an advantage of using *GIC* index stands also in the results obtained by Marshall et al. [2012] who, using a probabilistic approach on a very large number of worldwide occurrences of known faults, as malfunctioning and ruptures of transformers, quantified the threat to power systems in terms of *GIC* index and established a scale of the risk level from "low" to "extreme". Therefore, an accurate modelling of the dependence of *GIC* index maximum value with latitude could be used to assess the risk level of each country based on their geomagnetic latitude.

ACKNOWLEDGEMENTS

The results presented in this paper rely on data collected at magnetic observatories. We thank the national institutes that support them and INTERMAGNET for promoting high standards of magnetic observatory practice (www.intermagnet.org). Rapid magnetic variations are those calculated and made available by Ebre Observatory from data collected at magnetic observatories and on geomagnetic indices calculated and made available by ISGI Collaborating Institutes. We thank also the data suppliers and the WDC for Geomagnetism (Edinburgh) and the use of NASA/GSFC's Space Physics Data Facility's OMNIWeb (or CDAWeb or ftp) service, and OMNI data. The authors are grateful to two anonymous referees for their constructive reviews.

REFERENCES

Adebesin B.O., Pulkkinen, A. and Ngwira, C.M. (2016). The interplanetary and magnetospheric causes of extreme dB/dt at equatorial locations. Geophysical Research Letters, 43: 11, 501-11, 509, doi: 10.1002/2016GL071526.

Alekseev, D., Kuvshinov, A. and Palshin, N. (2015). Compilation of 3D global conductivity model of the Earth for space weather applications. Earth, Planets and Space, 67: 108, doi: 10.1186/s40623-015-0272-5.

Alken, P., and Maus, S. (2007). Spatio-temporal characterization of the equatorial electrojet from CHAMP, Ørsted, and SAC-C satellite magnetic measurements. J. Geophys. Res., 112: A09305, doi:10.1029/2007JA012524.

Carter, B.A., Yizengaw, E., Pradipta, R., Halford, A.J., Norman, R. and Zhang, K. (2015). Interplanetary shocks and the resulting geomagnetically induced currents at the equator. Geophys. Res. Lett., 42: 6554-6559, doi:10.1002/2015GL065060.

Carter, B.A., Yizengaw, E., Pradipta, R., Weygand, J.M., Piersanti, M., Pulkkinen, A., Moldwin, M. B., Norman, R. and Zhang, K. (2016). Geomagnetically induced currents around the world during the 17 March 2015 storm, J. Geophys. Res. Space Physics, 121: 10,496–10,507, doi:10.1002/2016JA023344.

de Villiers, J.S., Kosch, M. , Yamazaki, Y. and Lotz, S. (2017). Influences of various magnetospheric and ionospheric current systems on geomagnetically induced currents around the world, Space Weather, 15: 403–417, doi:10.1002/2016SW001566.

Farrugia, C. J., Jordanova, V.K.M., Thomsen, F., Lu, G., Cowley, S.W.H. and Ogilvie K.W. (2006). A two-ejecta event associated with a two-step geomagnetic storm. J. Geophys. Res., 111: A11104, doi:10.1029/2006JA011893.

Fiori, R.A.D., Boteler, D.H. and Gillies, D.M. (2014). Assessment of GIC risk due to geomagnetic sudden commencements and identification of the current systems responsible, Space Weather, 12: 76–91, doi:10.1002/ 2013SW000967.

Gaunt, C.T. and Coetzee, G. (2007). Transformer failures in regions incorrectly considered to have low GIC-risk. In Power Tech, 807-812, Inst. of Elect. and Electron. Eng., Lausanne, Switzerland.

Green, D. L., Waters, C.L., Anderson, B.J. and Korth, H. (2009). Seasonal and interplanetary magnetic field dependence of the field-aligned currents for both Northern and Southern Hemispheres. Ann. Geophys., 27: 1701–1715, doi:10.5194/angeo-27-1701-2009.

Hejda, P. and Bochníček, J. (2005). Geomagnetically induced pipe-to-soil voltages in the Czech oil pipelines during October-November 2003. Annales Geophysicae, 23: 3089--3093, SRef-ID:1432-0576/ag/2005-23-3089.

Iyemori, T. (1990). Storm-time magnetospheric currents inferred from mid-latitude geomagnetic field variations, J. Geomag. Geoelectr., 42: 1249–1265.

King, J.H. and Papitashvili, N.E. (2005). Solar wind spatial scales in and comparisons of hourly Wind and ACE plasma and magnetic field data. J. Geophys. Res., 110: A02104.

Lotko, W. (2017). The Unifying Principle of Coordinated Measurements in Geospace Science, Space Weather, 15: 553–557, doi:10.1002/2017SW001634.

Love, J.J. and Chulliat, A., (2013). An international network of magnetic observatories, *Eos Trans. AGU*, *94*: 373–374, doi:10.1002/2013EO420001.

Marshall, R.A., Waters, C.L. and Sciffer, M.D. (2010). Spectral analysis of pipe-to-spoil potentials with variations of the Earth's magnetic field in the Australian region. Space Weather, 8: S05002, doi: 10.1029/2009SW000553.

Marshall, R.A., Smith, E.A., Francis, M.J., Waters, C.L. and Sciffer, M.D. (2011). A preliminary risk assessment of the Australian region power network to space weather. Space Weather, 9: S10004, doi:10.1029/2011SW000685.

Marshall, R.A., Dalzell, M., Waters, C.L., Goldthorpe, P. and Smith, E.A. (2012). Geomagnetically induced currents in the New Zealand power network. Space Weather, 10: S08003, doi:10.1029/2012SW000806.

Mc Granaghan, R., Knipp, D.J., Matsuo, T. and Cousins, E. (2016). Optimal interpolation analysis of high-latitude ionospheric Hall and Pedersen conductivities: Application to assimilative ionospheric electrodynamics reconstruction. . Geophys. Res., 121: 4898-4923, doi: 10.1002/2016JA022486.

Moldwin, M.B. and Tsu J.S. (2016). Stormtime Equatorial Electrojet Ground-Induced Currents, in Increasing Power Grid Space Weather Impacts at Equatorial Latitudes, eds T. Fuller-Rowell, E. Yizengaw, P. H. Doherty and S. Basu, AGU Geophysical Monograph Series, doi:10.1002/9781118929216.ch3.

Molinski, T. S. (2002). Why utilities respect geomagnetically induced currents. J. Atmos. Sol. Terr. Phys., 64: 1765–1778, doi:10.1016/S1364-6826(02)00126-8.

Ngwira, C. M., Pulkkinen, A., Wilder, F. D. and Crowley, G. (2013). Extended study of extreme geoelectric field event scenarios for geomagnetically induced current applications. Space Weather, 11: 121-131, doi:10.1002/swe.20021.

Ngwira, C.M. and Pulkkinen, A.A. (2018). An Overview of Science Challenges Pertaining to Our Understanding of Extreme Geomagnetically Induced Currents, Chapter 8 in Extreme Events in Geospace: Origins, Predictability, and Consequences, Editor Natalia Buzulukova, 187–208, https://doi.org/10.1016/B978-0-12-812700-1.09992-1, Elsevier, Amsterdam.

Pirjola, R. (1982). Electromagnetic induction in the Earth by a plane wave or by fields of line currents harmonic in time and space. Geophysica, 18: 1-161.

Pirjola, R. (2002). Review on the calculation of surface electric and magnetic fields and of geomagnetically induced currents in ground-based technological systems. Surv. Geophys., 23: 71–90, doi:10.1023/A:1014816009303.

Prölss, G. (2004). Physics of the Earth's Space Environment, 513 pp, Springer.

Pulkkinen, A., Bernabeu, E., Eichner, J., Beggan, C. and Thomson, A.W.P. (2012). Generation of 100-year geomagnetically induced current scenarios. Space Weather, 10: S04003, doi:10.1029/2011SW000750.

Rabiu, A.B., Folarin, O.O., Uozumi, T., Hamid, N.S.A. Yoshikawa, A., (2017). Longitudinal variation of equatorial electrojet and the occurrence of its counter electrojet. Ann. Geophys., 35: 535–545, doi:10.5194/angeo-35-535-2017.

Smith, A.R.A., Beggan, C.D., Macmillan, S. and Whaler, K.A. (2017). Climatology of the auroral electrojets derived from the along-track gradient of magnetic field intensity measured by POGO, Magsat, CHAMP, and Swarm. Space Weather, 15: 1257–1269, doi:10.1002/2017SW001675.

Thomson, A.W.P., Gaunt, C.T., Cilliers, P., Wild, J.A., Opperman, B., McKinnell, L.-A., Kotze, P., Ngwira, C.M. and Lotz, S.I. (2010). Present day challenges in understanding the geomagnetic hazard to national power grids. Advances in Space Research, 45: 1182-1190, doi: 10.1016/j.asr.2009.11.023.

Tsuji, Y., Shinbori, A., Kikuchi, T. and Nagatsuma, T. (2012). Magnetic latitude and local time distributions ofionospheric currents during a geomagnetic storm. J. Geophys. Res., 117: A07318, doi:10.1029/2012JA017566.

Watari, S., Kunitake, M., Kitamura, K., Hori, T., Kikuchi, T., Shiokawa, K., Nishitani, N., Kataoka, R., Kamide, Y., Aso, T., Watanabe, Y. and Tsuneta, Y. (2009). Measurements of geomagnetically induced current in a power grid in Hokkaido, Japan. Space Weather, 7: S03002, doi:10.1029/2008SW000417.